20th AIAA Computational Fluid Dynamics Conference
27 - 30 June 2011, Honolulu, Hawaii

AIAA 2011-3407

Navier-Stokes Solution Using Hybridizable Discontinuous Galerkin methods

D. Moro*, N. C. Nguyen†, and J. Peraire‡
Massachusetts Institute of Technology, Cambridge, MA 02139, USA

We are concerned with the numerical solution of the Navier-Stokes and Reynolds-averaged Navier-Stokes equations using the Hybridizable Discontinuous Galerkin (HDG) methods recently introduced in Ref. [34]. These methods are computationally more efficient and accurate than other discontinuous Galerkin methods and hence, well suited to be applied to CFD problems. However, in order for them to be able to deal with the range of problems of relevance to Aeronautics, both turbulence and shocks have to be properly addressed. First, we will present a modification of the Spalart-Allmaras (SA) turbulence model that improves the convergence properties of the method by means of a regularization of the working variable; this modification is effective only in regions where the eddy viscosity is smaller than the molecular viscosity, therefore, it does not affect the numerical prediction of flow quantities as compared to the original SA model. Then, an artificial viscosity coefficient driven by the divergence of the velocity will be implemented in order to deal with shock waves. Numerical results are presented to demonstrate the proposed approach in several instances, from laminar separated flows to turbulent compressible flows.

I. Introduction

The numerical simulation of viscous compressible flows has become an indispensable tool for many important applications such as aero-acoustics, vehicle design and turbomachinery. Although the ever increasing computer power allows us to solve complex problems that would have been intractable a few years ago, there are still many problems of practical interest for which the existing methods are inadequate. Therefore, the development of robust, accurate, and efficient methods for the numerical solution of the compressible Navier-Stokes equations in complex geometries remains a topic of considerable importance. In particular, we are concerned with the solution of flows where shock waves are present and the Reynolds number is high enough so that some sort of turbulence modeling is required. To do so, the Reynolds Averaged Navier-Stokes system (RANS) combined with the one equation Spalart-Allmaras (SA) model with transition terms will be used. In order to tackle this system the hybridizable discontinuous Galerkin (HDG) method, recently introduced in Ref. [34], will be applied. In addition to possessing local conservativity, high-order accuracy, and strong stability for convection-dominated flows, the HDG methods have the following main advantages over many existing DG methods. First, unlike other DG methods which result in a final system involving the degrees of freedom of the approximate field variables, the HDG methods produce a final system in terms of the degrees of freedom of the *approximate traces* of the field variables. Since the approximate traces are defined on the element faces only and single-valued on every face, the HDG methods have significantly less globally coupled unknowns than other DG methods. This large reduction in the degrees of freedom can lead to significant savings for both computational time and memory storage. Second, for diffusion-dominated problems with smooth solutions, the HDG methods exhibit optimal convergence properties for the primal variables as well as their gradients. In fact, to our knowledge, it is the only DG method that achieves optimal convergence of the viscous fluxes in multidimensions. Finally, the HDG methods can deal with inflow, outflow, slip, and solid wall boundary conditions weakly in a unified framework by defining appropriate numerical fluxes on the domain boundaries.

*PhD Candidate, Department of Aeronautics and Astronautics, M.I.T., 77 Massachusetts Avenue, AIAA Student Member.
†Research Scientist, Department of Aeronautics and Astronautics, M.I.T., 77 Massachusetts Avenue, AIAA Member.
‡Professor, Department of Aeronautics and Astronautics, M.I.T., 77 Massachusetts Avenue, AIAA Associate Fellow.

The first HDG method was introduced for diffusion-reaction problems[11] and later analyzed in.[7,13,14] Several HDG methods were subsequently developed for biharmonic equations,[8] linear and nonlinear convection-diffusion problems,[9,28,29] linear elasticity,[39] Stokes flows,[10,12,15,30] incompressible Navier-Stokes equations,[26,27,31] compressible Navier-Stokes equations,[34] linear acoustic and elastodynamics,[25] and time-harmonic Maxwell's equations.[24] Although HDG methods are locally conservative and stable for convection-dominated flows, they produce oscillatory solutions in the presence of shock waves. These oscillations known as the Gibbs phenomenon will eventually preclude convergence of the simulation. In the literature, several techniques such as filters, limiters, reconstruction, and artificial viscosity have been proposed to suppress oscillations around the discontinuities. The approach we have taken here relies on artificial viscosity as a way to stabilize the solution around discontinuities. In [32], we introduce an artificial viscosity model for the compressible Euler equations. In this paper, we extend this artificial viscosity method to viscous compressible flows.

Artificial viscosity has been widely used in finite volume methods,[23] streamline upwind Petrov-Galerkin (SUPG) methods,[22] and spectral methods.[40] Recently, DG researchers have also employed artificial viscosity to capture shocks. Hartmann and Houston[21] used the magnitude of the residual to determine the amount of viscosity added around the shock region. Persson and Peraire[35] introduced a sub-cell shock-capturing method based on the smoothness of an orthogonal expansion of the computed density for determining the shock region and amount of artificial viscosity added there. However, a drawback of this approach is that it may lead to oscillations in state gradients because the artificial viscosity is piecewise-constant. Recognizing this limitation by the Persson and Peraire's approach, Barter and Darmofal introduced a PDE-based artificial viscosity model[2] appended to the system of governing equations to obtain smoother gradients. However, the PDE-based artificial viscosity approach is clearly more expensive since it solves an additional PDE to be solved for. Yet another approach proposed by Cook and Cabot[16–18] consists of adding artificial terms to the physical viscosity coefficients such as the dynamic viscosity, bulk viscosity, and thermal conductivity. The added artificial terms are determined based on the strain rate tensor and the internal energy. This approach was followed up with the work by Lele et al.[5,19] in the context of compressible turbulence simulations. The approach was also adopted by Premasuthan et al.[36] for spectral difference method.

Regarding turbulence modeling, it is well known that the development of high-order methods for the solution of the RANS equations coupled with a turbulence closure model is a challenging task because of the stiffness associated to the closure equations. In practice, it is often necessary to supplement the turbulence model with some form of stabilization to prevent the divergence of the simulations. In the previous work,[33] we proposed to add artificial dissipation into the Spalart-Allmaras (SA) turbulence model in order to avoid oscillations and negative values of the eddy viscosity along the edge of the boundary layer. In this paper, we take a different approach by pursuing a simple modification of the SA equation in order to render it easier to integrate using high-order methods. The modification is indeed necessary to avoid the sudden divergence often experienced when HDG is applied to the original SA model. We aim to explain why the blow-ups may occur and propose a fix to prevent them. In fact, our modification is effective only in regions where the eddy viscosity is smaller than the molecular viscosity. Therefore, it does not affect the numerical prediction of flow quantities as compared to the original SA model.

II. Flow Models

In this section, the different models used (RANS, SA, and Artificial Viscosity) will be described separately. For the sake of clarity, the HDG implementation of the final system of equations will not be described here; the interested reader is referred to [34] for details on the implementation of the Navier-Stokes equations such as the underlying weak formulation, the boundary conditions, etc. or any of the references provided in the introduction above.

A. Navier-Stokes and RANS Equations

We consider the compressible Navier-Stokes equations

$$\frac{\partial \rho}{\partial t} + \frac{\partial \rho u_j}{\partial x_j} = 0 \tag{1}$$

$$\frac{\partial}{\partial t}(\rho u_i) + \frac{\partial}{\partial x_j}(\rho u_i u_j) + \frac{\partial p}{\partial x_i} - \frac{\partial \tau_{ji}}{\partial x_j} = 0 \tag{2}$$

$$\frac{\partial}{\partial t}(\rho E) + \frac{\partial}{\partial x_j}(u_j(\rho E + p)) - \frac{\partial}{\partial x_j}(u_i \tau_{ji}) + \frac{\partial q_j}{\partial x_j} = 0 \tag{3}$$

$$p = (\gamma - 1)\rho(E - u_k^2/2) \tag{4}$$

$$q_j = -\frac{\mu}{Pr}\frac{\partial}{\partial x_j}(E + p/\rho - u_k^2/2) \tag{5}$$

$$\tau_{ij} = \mu\left[\frac{\partial u_i}{\partial x_j} + \frac{\partial u_j}{\partial x_i} - \frac{2}{3}\frac{\partial u_k}{\partial x_k}\delta_{ij}\right] \tag{6}$$

where γ, Pr and μ are the ratio of gas specific heats, the molecular Prandtl number and molecular dynamic viscosity, respectively.

The Reynolds averaged Navier-Stokes (RANS) equations are obtained from the Navier-Stokes equations by means of an averaging process that introduces the so called Reynolds stresses $\overline{u_i' u_j'}$. If the Bousinesq eddy viscosity assumption is invoked, then the Reynolds stresses are modeled as being proportional to the mean strain rate tensor. That way the Reynolds stresses are included in system 1-6 by simply replacing μ with $\mu + \mu_t$, where μ_t is the turbulent dynamic viscosity. Similarly, the heat transfer coefficient μ/Pr has to be replaced by $\mu/Pr + \mu_t/Pr_t$. This is:

$$q_j = -\left(\frac{\mu}{Pr} + \frac{\mu_t}{Pr_t}\right)\frac{\partial}{\partial x_j}(E + p/\rho - u_k^2/2) \tag{7}$$

$$\tau_{ij} = (\mu + \mu_t)\left[\frac{\partial u_i}{\partial x_j} + \frac{\partial u_j}{\partial x_i} - \frac{2}{3}\frac{\partial u_k}{\partial x_k}\delta_{ij}\right] \tag{8}$$

To close the system of equations 1-6, the eddy viscosity μ_t and the turbulent Prandtl number Pr_t have to be modeled. For the former, a modified version of the Spalart-Allmaras one equation model is used in order to trace the evolution of the eddy viscosity in the domain. As for Pr_t, we are interested in low to moderate speed flows with negligible heat transfer effects, hence a constant value of $Pr_t = 0.9$ is a reasonable approximation.

B. The Spalart-Allmaras Model

In the Spalart-Allmaras model,[38] a working variable $\tilde{\nu}$ is solved together with the RANS equations subject to the following governing transport law:

$$\frac{D\tilde{\nu}}{Dt} = c_{b1}\tilde{S}\tilde{\nu} + \frac{1}{\sigma}\left[\nabla\cdot\left((\nu + \tilde{\nu})\nabla\tilde{\nu}\right) + c_{b2}\left(\nabla\tilde{\nu}\right)^2\right] - c_{w1}f_w\left[\frac{\tilde{\nu}}{d}\right]^2 \tag{9}$$

where the three different terms on the right hand side represent turbulence production due to shear, turbulence diffusion/propagation into the flow and turbulence destruction due to walls, respectively. The effective eddy viscosity applied to the RANS system is computed from $\tilde{\nu}$ as follows:

$$\mu_t = \rho\nu_t, \qquad \nu_t = \tilde{\nu}f_{v1}, \qquad f_{v1} = \frac{\chi^3}{\chi^3 + c_{v1}^3}, \qquad \chi = \frac{\tilde{\nu}}{\nu}\ . \tag{10}$$

while the production term takes the form:

$$\tilde{S} = S + \frac{\tilde{\nu}}{\kappa^2 d^2}f_{v2}\ , \tag{11}$$

$$S = \sqrt{2\Omega_{ij}\Omega_{ij}}, \qquad f_{v2} = 1 - \frac{\chi}{1 + \chi f_{v1}}\ . \tag{12}$$

Here $\Omega_{ij} = \frac{1}{2}(\partial u_i/\partial x_j - \partial u_j/\partial x_i)$ is the rotation tensor and d is the distance from the closest wall. Finally, the destruction term is given by:

$$f_w = g\left[\frac{1 + c_{w3}^6}{g^6 + c_{w3}^6}\right]^{1/6}\ , \tag{13}$$

$$g = r + c_{w2}(r^6 - r), \qquad r = \frac{\tilde{\nu}}{\tilde{S}\kappa^2 d^2}\ . \tag{14}$$

The closure constants involved in the model are set as follows: $c_{b1} = 0.1355$, $c_{b2} = 0.622$, $c_{v1} = 7.1$, $\sigma = 2/3$, $c_{w1} = \frac{c_{b1}}{\kappa^2} + \frac{(1+c_{b2})}{\sigma}$, $c_{w2} = 0.3$, $c_{w3} = 2$, $\kappa = 0.41$.

In order to model forced transition, the SA model has to be modified to make $\tilde{\nu} = 0$ a stable solution of the problem up to a desired threshold. This way, the solution can remain laminar up until certain locations where the system is perturbed out of equilibrium and the eddy viscosity starts evolving. To do so, the right hand side is modified so that when $\tilde{\nu}$ is small enough the linearized system is stable; for this, the leading term needs to have the shape $D\tilde{\nu}/Dt = \lambda\tilde{\nu}$ with $\lambda < 0$. The approach followed in the original work by Spalart and Allmaras[38] reads:

$$\frac{D\tilde{\nu}}{Dt} = c_{b1}(1 - f_{t2})\tilde{S}\tilde{\nu} + \frac{1}{\sigma}\left[\nabla \cdot ((\nu + \tilde{\nu})\nabla\tilde{\nu}) + c_{b2}(\nabla\tilde{\nu})^2\right] - (c_{w1}f_w - \frac{c_{b1}}{\kappa^2}f_{t2})\left[\frac{\tilde{\nu}}{d}\right]^2 + f_{t1}\Delta U^2 \tag{15}$$

where the new functions are defined as:

$$f_{t1} = c_{t1}g_t \exp(-c_{t2}\frac{w_t^2}{\Delta U^2}[d^2 + g_t^2 d_t^2]), \qquad f_{t2} = c_{t3}\exp(-c_{t4}\chi^2), \tag{16}$$

Here, d_t represents the distance to the trip, w_t represents the vorticity at the trip, ΔU equals the difference in velocity between the fluid and the trip (this last usually zero) and $g_t = \min(0.1, \Delta U/w_t\Delta x)$. The constants in these terms are set to: $c_{t1} = 1$, $c_{t2} = 2$, $c_{t3} = 1.1$ and $c_{t4} = 2$.

With this choice of tripping functions and constants, the zero eddy viscosity solution is stable up to $\chi \approx 0.14$ and is pushed out of equilibrium by the f_{t1} function. More details on this can be found in the original reference.[38] The free-stream condition is set to $\tilde{\nu} = \nu/10$ in order to be consistent with the stabilization terms. In cases where the interest lies on fully turbulent solutions, the trip terms can be neglected and the free-stream value for the working variable can be set to $\tilde{\nu} = \nu$. In any case, the boundary condition for the working variable at solid walls is $\tilde{\nu} = 0$.

C. Modification of the Spalart-Allmaras Model

It is well known that high order methods face a series of challenges when it comes to solving the RANS equations, all of them associated to the stiffness of the equations that govern the eddy viscosity evolution.[3,33] In particular, for the SA model, the weak solution corresponding to the propagation of turbulence into the laminar region (due to the diffusion term $\nabla \cdot (\tilde{\nu}\nabla\tilde{\nu})$) is discontinuous in the first derivative and only regularized by the effect of the molecular viscosity ($\nabla\cdot((\nu+\tilde{\nu})\nabla\tilde{\nu})$). It is thus clear that in situations where the length scale of the molecular viscosity is much smaller than the resolution, the high order approximation (polynomials in the case of HDG) will suffer from oscillations due to the discontinuity; these can later trigger two other problems, namely:

1. In the case where the resolution at the edge of the boundary layer is too small, the oscillation in $\tilde{\nu}$ can be negative enough to reach $\chi = -c_{v1}$, in which case the function f_{v1} becomes unbounded and a sudden blow-up in the computation is experienced.

2. Even though such small values are not reached, it is enough to reach $\chi = -c_{v1}/\sqrt[3]{2}$ to cancel the molecular viscosity applied to the RANS equations. Furthermore, values of $\chi < -1$ produce negative total viscosity in the SA model. In short, below a certain threshold, negative χ can turn dissipative terms into anti-dissipative ones.

To address the above issues we propose a simple modification of the SA model consisting on a transformation that avoids $\chi < 0$. In particular, we replace χ with

$$\psi = 0.05\log\left(1 + \exp\left(20\chi\right)\right) \tag{17}$$

As plotted in Figure 1, ψ is almost identical to χ for $\tilde{\nu} \geq \nu$. In fact, the difference $|\psi - \chi|$ is smaller than 1.04×10^{-10} for $\tilde{\nu} \geq \nu$ and just over 1.5% for $\tilde{\nu} = 0$. However, unlike χ which goes negative, ψ vanishes rapidly to zero for negative values of the working variable. As a result, if ψ is used as argument for f_{v1}, the turbulent eddy viscosity applied to the RANS equations can never be negative. Similarly, if $\psi\nu$ instead of $\tilde{\nu}$ is used in the diffusion term of the SA model, the dissipative character of the operator is always preserved. Our proposed modification is to use the regularized ψ instead of χ wherever possible. The modified model reads:

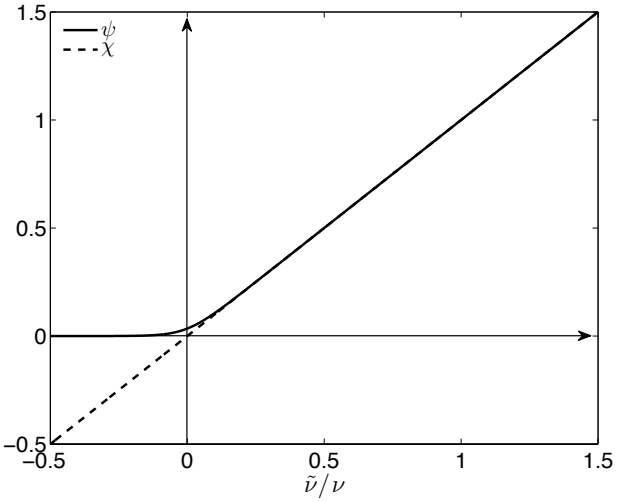

Figure 1: Plots of ψ and χ as a function of $\tilde{\nu}/\nu$.

$$\frac{D\tilde{\nu}}{Dt} = c_{b1}(1-f_{t2})\tilde{S}\psi\nu + \frac{1}{\sigma}\left[\nabla\cdot\left(\left(\nu+\psi\nu\right)\nabla\tilde{\nu}\right) + c_{b2}\left(\nabla\tilde{\nu}\right)^2\right] - \left(c_{w1}f_w - \frac{c_{b1}}{\kappa^2}f_{t2}\right)\left[\frac{\psi\nu}{d}\right]^2 + f_{t1}\Delta U^2 \tag{18}$$

where the different functions involved are defined as:

$$\tilde{S} = S + \frac{\psi\nu}{\kappa^2 d^2}f_{v2}, \qquad S = \sqrt{2\Omega_{ij}\Omega_{ij}}, \qquad f_{v1} = \frac{\psi^3}{\psi^3 + c_{v1}^3}, \qquad f_{v2} = 1 - \frac{\psi}{1+\psi f_{v1}} \tag{19}$$

$$f_w = g\left[\frac{1+c_{w3}^6}{g^6+c_{w3}^6}\right]^{1/6}, \qquad g = r + c_{w2}(r^6 - r), \qquad r = \frac{\psi\nu}{\tilde{S}\kappa^2 d^2}\ . \tag{20}$$

and the trip terms (f_{t1} and f_{t2}) are not modified and still depend on χ in the case of f_{t2}. The turbulent dynamic viscosity is then calculated as

$$\mu_t = \rho\nu_t, \qquad \nu_t = \psi\nu f_{v1}, \qquad f_{v1} = \frac{\psi^3}{\psi^3 + c_{v1}^3}\ . \tag{21}$$

The closure constants used in the original SA model where obtained out of a careful calibration for several canonical cases under the hood of second order finite difference schemes. This calibration seems to be still valid when high order methods on sufficiently fine meshes are used,[33] however, the modification we propose introduces subtle changes, specially for small or negative $\tilde{\nu}$ that might slightly modify the parameters of the model. In any case, our main goal is to asses the enhanced stability of the proposed modification and hence a re-calibration will not be carried out here.

It is important to point out that our modification does not aim to alleviate the issue of negative working variable $\tilde{\nu}$ in the SA model. In particular, this variable may still be negative if the boundary layer edge is under-resolved. However, the modification is beneficial for high-order methods since it renders the resulting system easier to integrate. We observe from our numerical experiments that the modified SA model succeeds in a number of cases where the original SA model fails.

D. Shock Capturing

In order to treat shock waves, the Navier-Stokes or RANS equations have to be written in non-dimensional conservation form as:

$$\frac{\partial \boldsymbol{u}}{\partial t} + \nabla\cdot\left(\boldsymbol{F}(\boldsymbol{u},\nabla\boldsymbol{u}) - \varepsilon\nabla\tilde{\boldsymbol{u}}\right) = 0, \tag{22}$$

where $\boldsymbol{u}$ is the m-dimensional vector of conserved dimensionless quantities and $\boldsymbol{F}(\boldsymbol{u}, \nabla \boldsymbol{u})$ are the *physical* fluxes of dimension $m \times d$, that have been augmented by the *artificial* fluxes $\varepsilon \nabla \tilde{\boldsymbol{u}}$ of dimension $m \times d$ too. The later are added to the original equations for the purpose of capturing shocks. Here ε is the artificial viscosity and $\tilde{\boldsymbol{u}}$ is the same as $\boldsymbol{u}$ except that the energy is replaced with the enthalpy.[2]

Following the previous work,[5,36] we define the artificial viscosity as

$$\varepsilon = \varepsilon_0 f\Big(\frac{\ell \nabla \cdot \boldsymbol{v}}{c}\Big), \tag{23}$$

where ε_0 is a user-specified constant, ℓ is a characteristic length scale, $\boldsymbol{v}$ is the velocity field, $c = \sqrt{\gamma p/\rho}$ is the sound speed, and f is an analytic function. Not wanting to add viscosity at the wall, we specify ℓ as

$$\ell = \min(h_0, 10 d_w), \tag{24}$$

where h_0 is a representative size of the finite elements and d_w is the distance from the closest wall. To complete our artificial viscosity model we define f as

$$f(x) = \alpha \log(1 + \exp((\beta - x)/\alpha)), \tag{25}$$

where $\alpha = 0.05$ and $\beta = -0.5$. The function f plays the same role as the regularization introduced for the SA model. In this case though, the objective is to apply artificial viscosity when the divergence of the velocity is negative (compressive data) and cannot be resolved in the available length scale (ℓ/c). As a result, the artificial viscosity added is continuous within each element. The jumps in artificial viscosity between elements are related to the jumps in the solution at the interface, and hence, will tend to zero if the solution is properly resolved. This way, the concerns associated to the artificial viscosity being a constant inside the element[2,35] instead of a field itself no longer apply.

III. Results

In this section, some results obtained using HDG and the previous models will be presented. The objective is to show the capabilities of this approach in different flow regimes; from laminar separated to turbulent transonic flows.

A. Laminar flow past SD7003 foil

We first consider the laminar flow past a SD7003 at low Reynolds number. It is well known that this airfoil presents a laminar separation bubble that can experience reattachment if transition occurs. However, our interest lies on the laminar separation regime and the associated vortex shedding.

Figure 2 shows a snapshot of the horizontal velocity and vorticity as obtained using HDG for $Re = 10^4$, $M_\infty = 0.2$, and $\alpha = 4^o$. In this case, the solution is computed on a C-mesh of 3360 triangular elements using polynomials of order p=4 and time integration is carried out using a third order accurate DIRK scheme with time step $\Delta t = 0.025$. We observe the typical vortex structures shedding behind the airfoil, that compares well with the results reported by Uranga et al using LES .[41] Notice how the combination of accurate time stepping and spatial discretization yields a solution with small dissipation that can capture the vortex propagation into the wake with high fidelity.

B. Turbulent flow over flat plate

The next set of results deals with the turbulent flow over a flat plate, that represents the simplest tests case for the validation of the modified SA model due to the simplicity of the geometry and the availability of experimental data.[6] The case studied here consists on a flat plate at $M_\infty = 0.2$ and $Re = 1.027 \cdot 10^7$. In order to compute the solution, the modified SA model is used without the trip terms on a mesh consisting on 572 triangles and polynomial order $p = 2$ to $p = 4$. The first high order node off the wall is placed at a distance $y/L = 2.75 \cdot 10^{-5}$ while the first node over the flat plate is placed at $x/L = 2.37 \cdot 10^{-3}$ from the leading edge.

The results for this case are plotted in Figure 3 and show the value of the SA working variable as well as the velocity profile (non dimensionalized with u_τ and ℓ_τ) for different polynomial orders. The results agree

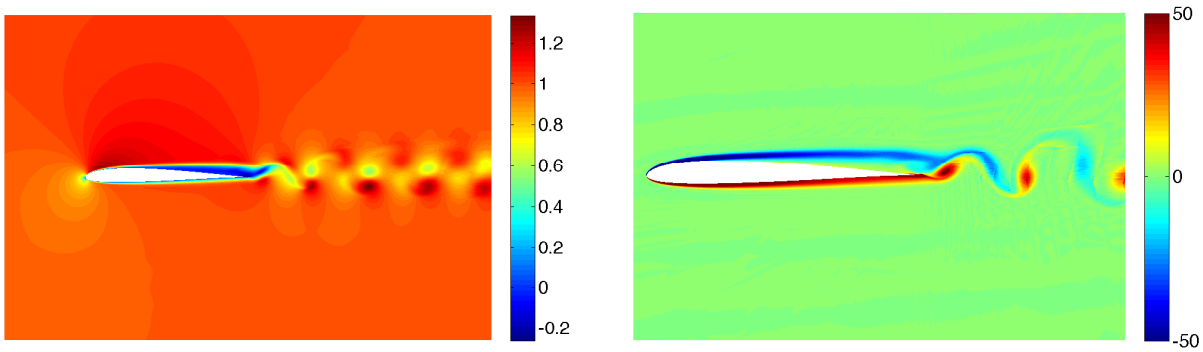

(a) Horizontal Velocity

(b) Vorticity

Figure 2: Snapshot of the horizontal velocity u (left) and vorticity ω (right) for laminar flow past a SD7003 foil at $Re = 10^4$, $M_\infty = 0.2$, and $\alpha = 4^o$.

well with the experimental results[6] as well as the law of the wall. Notice the slight oscillation at the edge of the eddy viscosity boundary layer does not prevent the convergence towards a solution.

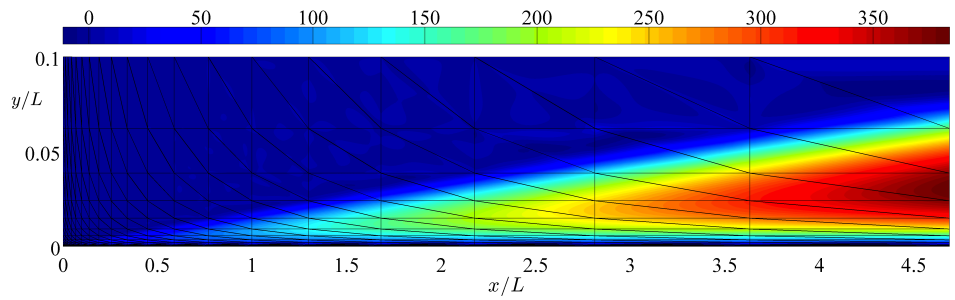

(a) SA working variable, $p = 4$

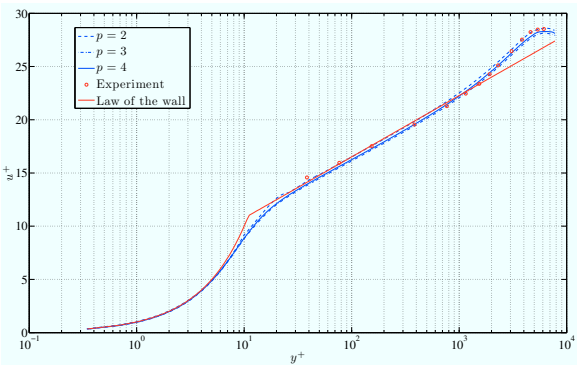

(b) Velocity profile

Figure 3: Relative value of the SA working variable $\chi = \tilde{\nu}/\nu$ (top) and velocity profile at $Re_x = 1.027 \cdot 10^7$ (bottom) for a flat plate at $M_\infty = 0.2$ and $Re = 1.027 \cdot 10^7$.

C. Transition to turbulence over flat plate

Following, we deal with the turbulent transition over a simple geometry, again, using a flat plate at $M_\infty = 0.2$ and $Re = 1.027 \cdot 10^7$. In order to compute the solution, the modified SA model is used with the trip terms included. The discretization is carried out using polynomials of order $p = 4$ and a grid of 952 triangles. The

first high order node off the wall is placed at a distance $y/L = 1.73 \cdot 10^{-5}$ while the first node over the flat plate is placed at $x/L = 7.86 \cdot 10^{-4}$ from the leading edge.

Tripping is prescribed to occur at a certain location (forced trip) and the value of vorticity there, required by the SA model, is obtained from the Blasius solution. The inclusion of a small laminar region helps alleviate the singularity present at the leading edge, plus, it is interesting on its own in order to asses the behavior of the transition mechanism in the SA model.

Before trying to solve the problem, we need to check the stability of the modified SA model. In particular, we need to check that the eddy viscosity is attracted to zero when the stabilization terms are active and the free-stream condition is set to be small, regardless of the shear present in the flow. For this, the solution is computed using a free-stream value for the SA working variable of $\tilde{\nu}/\nu = 0.1$. The results for the friction coefficient C_f along the plate and the velocity profile at the $x/L = 0.96$ station are included in Figure 4. As we can see, the friction coefficient follows the laminar Blasius law and the velocity profile presents the usual laminar shape. The value of the working variable in the final solution remains in the gap $\tilde{\nu}/\nu \in [-0.077, 0.1029]$ as desired. The oscillation in the C_f close to the leading edge is due to the boundary layer singularity together with lack of resolution and only affects the first two elements.

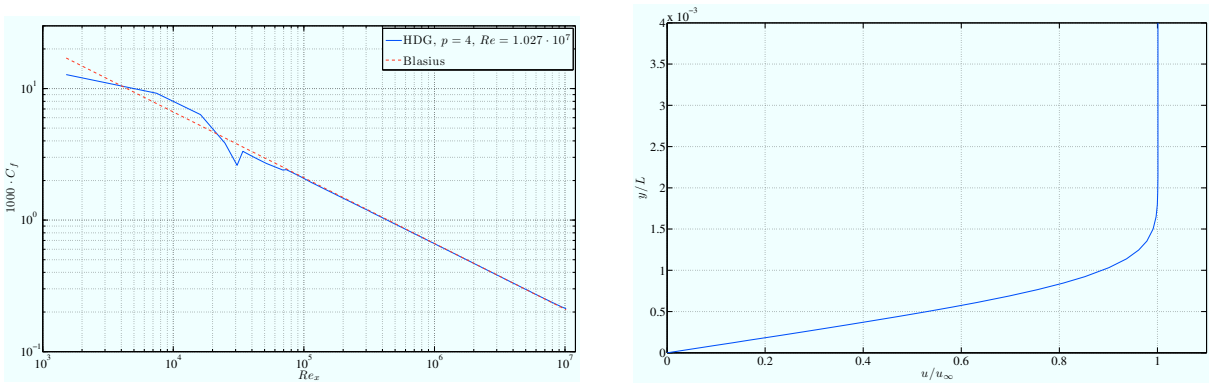

(a) Friction coefficient

(b) Velocity profile

Figure 4: Friction coefficient (left) and velocity profile (right) for the stabilized RANS laminar solution over a flat plate at $M_\infty = 0.2$ and $Re = 10^7$. The solution remains laminar throughout the flat plate which indicates the stabilization terms are working properly.

After checking the stability of the modified SA model, we are ready to solve the turbulent flow over the flat plate. For this, the trip is set to occur at $Re_x = 5 \cdot 10^5$ and the free-stream condition for the SA working variable is set to $\tilde{\nu}/\nu = 0.1$. In order to converge to a solution, time marching is mandatory. In this case, a second order, single stage Diagonally Implicit Runge-Kutta scheme has been used, with a prescribed growth in the time step length. This strategy requires several restarts and plenty of heuristics in the choice of the time step law. The method would definitely benefit from more robust strategies such as p-continuation and time step control through the CFL number.[4]

Figure 5 shows the computed solution for the friction coefficient over the flat plate obtained using the modified SA model. As we can see, the friction coefficient is in good agreement with usual laminar and turbulent fitting laws.[37] The solution computed setting the trip term parameter to $c_{t1} = 1.0$ presents an overshoot in the friction coefficient that might be alleviated if the trip strength was reduced. The corresponding result for $c_{t1} = 0.1$ does not present such overshoot and still produces the desired transition.

To complete the results, the horizontal velocity and the eddy viscosity fields close to the leading edge are included in Figure 6. Notice at the transition location (roughly at $x/L = 0.05$), the boundary layer profile smoothly changes and the eddy viscosity starts to grow as expected. Before this point, the boundary layer resembles the Blasius solution and the turbulence effects (through the eddy viscosity) are null. Notice also, the modified SA model we propose seems to be capable of dealing with transition within a single element.

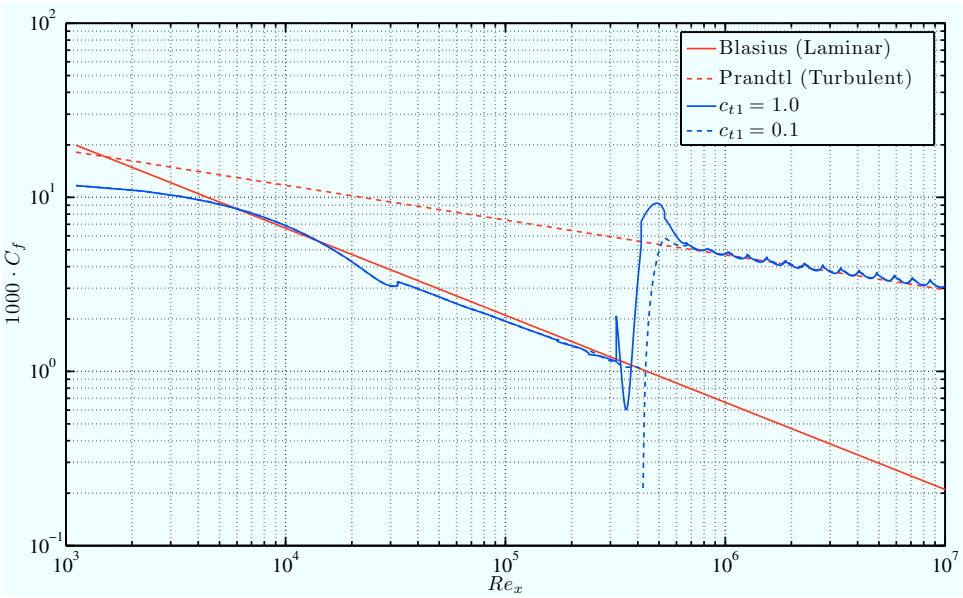

Figure 5: Friction coefficient over a flat plate at $M_\infty = 0.2$ and $Re = 1.027 \cdot 10^7$. Transition is forced to occur at $Re_x = 5 \cdot 10^5$. The result agrees well with laminar and turbulent friction laws.

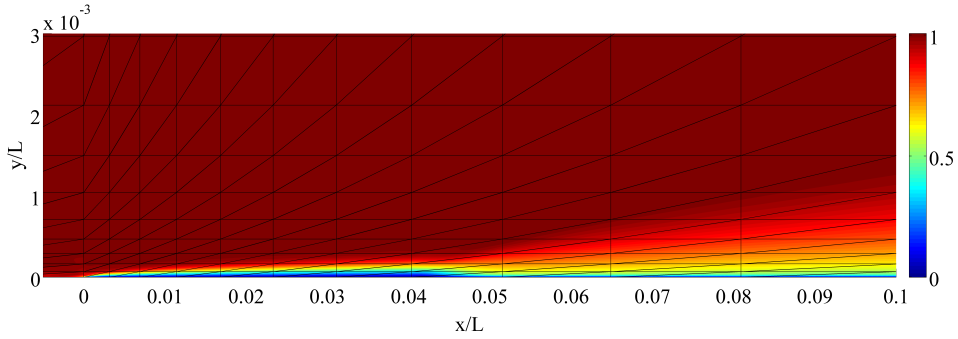

(a) Horizontal Velocity

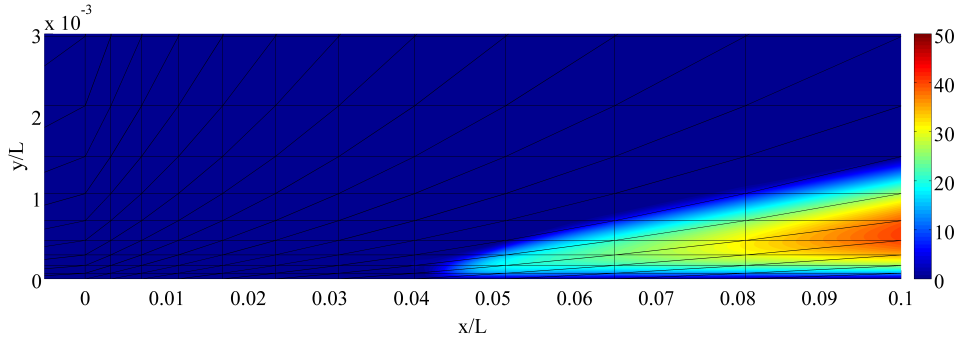

(b) Relative Eddy Viscosity

Figure 6: Horizontal velocity u (top) and relative SA working variable $\chi = \tilde{\nu}/\nu$ (bottom) in the region around the leading edge of a flat plate at $M_\infty = 0.2$ and $Re = 1.027 \cdot 10^7$. Transition is forced to occur at $Re_x = 5 \cdot 10^5$. Notice transition is produced smoothly within an element.

D. Turbulent subsonic flow past NACA 0012 foil

We next present results for the fully turbulent flow past NACA 0012 airfoil at Mach number $M_\infty = 0.3$, Reynolds number $Re = 1.85 \times 10^6$, and zero angle-of-attack . We use a single-block, two-dimensional C-grid of 101×31 nodes consisting on quadrilateral elements of order $p = 4$. The grid is clustered around the leading edge and the trailing edge to resolve the flow gradients there, and around the airfoil surface to resolve the boundary layer. The first high order node off the airfoil is at a distance of $d/c = 7 \times 10^{-6}$.

The problem was evolved in time from an initial uniform condition and convergence was achieved in around 40 iterations. Figure 7 shows the working variable field χ around the airfoil and in the wake. We can observe oscillations in the wake with χ as low as $\chi = -50$ due to the lack of resolution of the mesh there. Despite this, the convergence of the scheme was not affected; if the original SA model had been used in this same mesh, there would have been convergence issues due to this lack of resolution. Also, Figure 8 depicts the pressure coefficient distribution. We see that numerical predictions agree well with the experimental measurements.[1]

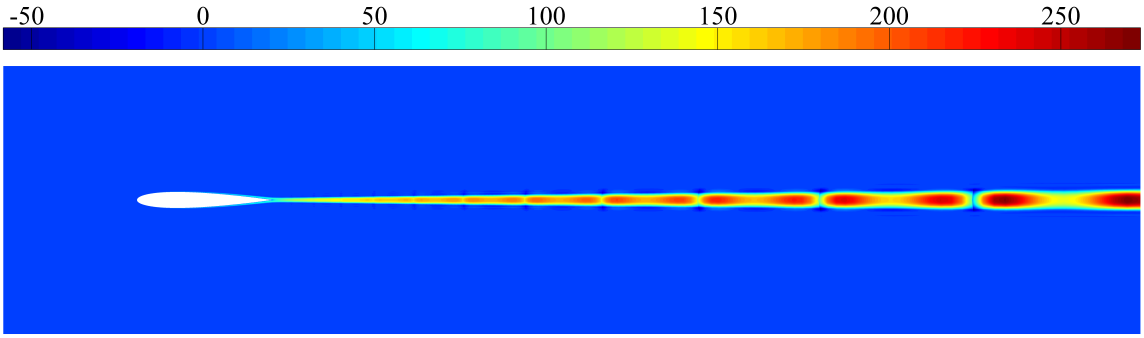

Figure 7: Relative SA working variable ($\chi = \tilde{\nu}/\nu$) solution for a turbulent subsonic flow past NACA 0012 airfoil at $M_\infty = 0.3$, $\alpha = 0^o$, and $Re = 1.85 \times 10^6$. Notice the under-resolution in the wake generates strong negative oscillations in the working variable that do not affect the modified SA model convergence.

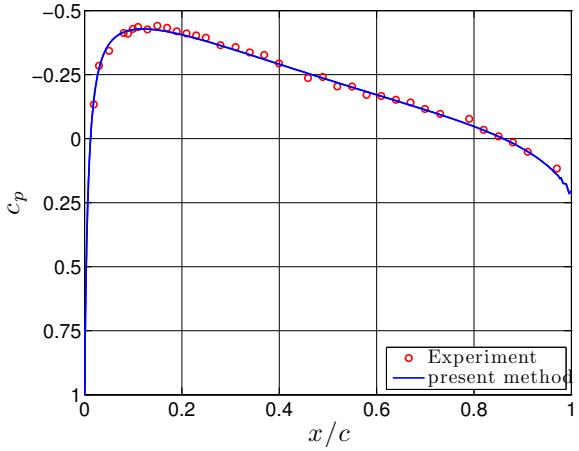

Figure 8: Pressure coefficient distribution over the airfoil surface for turbulent subsonic flow past NACA 0012 airfoil at $M_\infty = 0.3$, $\alpha = 0^o$, and $Re = 1.85 \times 10^6$.

E. Laminar Separation Bubble and transition on the SD7003 airfoil

All the previous results seem to indicate the proposed approach is adequate to deal with transition on attached flows and fully turbulent computations. However, we are also interested in cases where transition occurs in free shear layers and drastically modifies the flow field. One of this situations is the reattachment

that laminar separation bubbles can experience in the low-moderate Reynolds number regime. A well studied example of this would be the SD7003 airfoil, for which Large Eddy Simulation results exist.[20,41]

In this case, we are interested in the solution of the flow around the SD7003 airfoil at Mach number $M_\infty = 0.3$ and Reynolds number $Re = 60000$. The solution will be computed using a C-mesh of 864 quadrilateral elements with polynomial order $p = 4$. The modified SA model was used with the trip term parameters extracted from the results found in Uranga et al.[41] In particular, transition is set to occur at $x/c = 0.535$ and a distance $d/c = 0.025$ off the wall. No comparison with the results provided there are attempted because of the strong dependence of the solution on the trip parameters and the grid. For this, the results shown in Figures 9 and 10 for the pressure coefficient and the velocity field should be taken as merely qualitative. The solution exhibits a separation bubble on the upper surface that reattaches due to transition and produces the usual drop in the pressure coefficient.

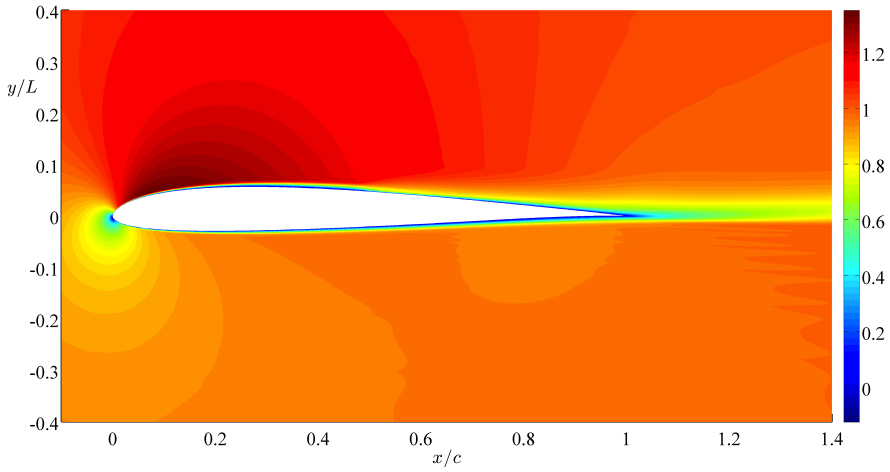

Figure 9: Horizontal velocity u for the flow around a SD7003 airfoil at $M_\infty = 0.3$, $\alpha = 4^o$, and $Re = 60000$. Notice the thin laminar separation bubble that reattaches around $x/c = 0.5$.

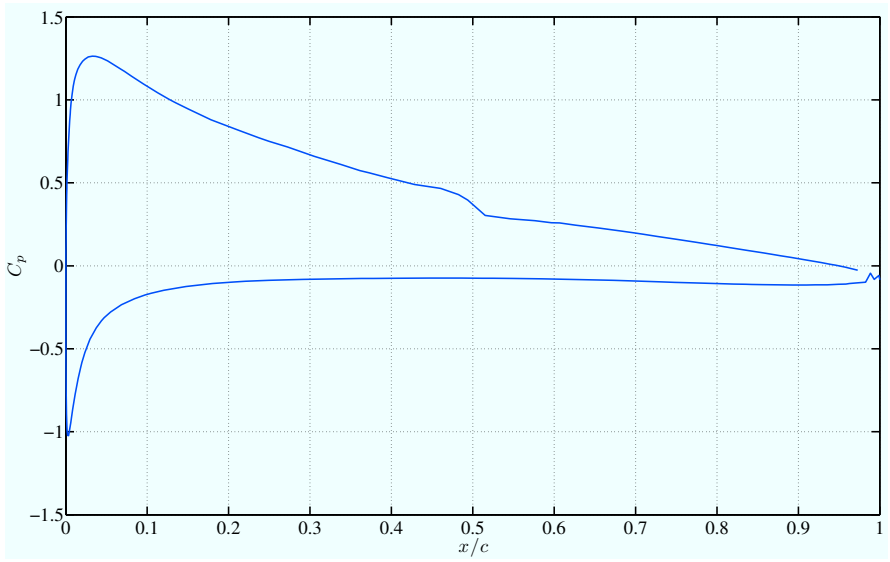

Figure 10: Pressure coefficient over an SD7003 airfoil at $M_\infty = 0.3$, $\alpha = 4^o$, and $Re = 60000$. Notice the drop due to the reattachment of the separation bubble following transition

F. Turbulent transonic flow past RAE 2822 foil

Finally, we present the results for a transonic turbulent flow on a RAE 2822 airfoil at free-stream Mach number $M_\infty = 0.729$, Reynolds number $Re = 6.5 \times 10^6$, and $\alpha = 2.31^o$ angle-of-attack. The goal of this test case is to explore the robustness of the proposed approach when combined with shock capturing.

The solution was computed on a C-mesh of 3456 triangular elements using polynomials of order $p = 4$. Figure 11 shows the pressure contour and the pressure coefficient distribution over the airfoil surface, that resembles the experimental results[1] except for the location of the shock. This may be due to the coarse mesh used and further studies would be required. Figure 12 shows the SA working variable field obtained.

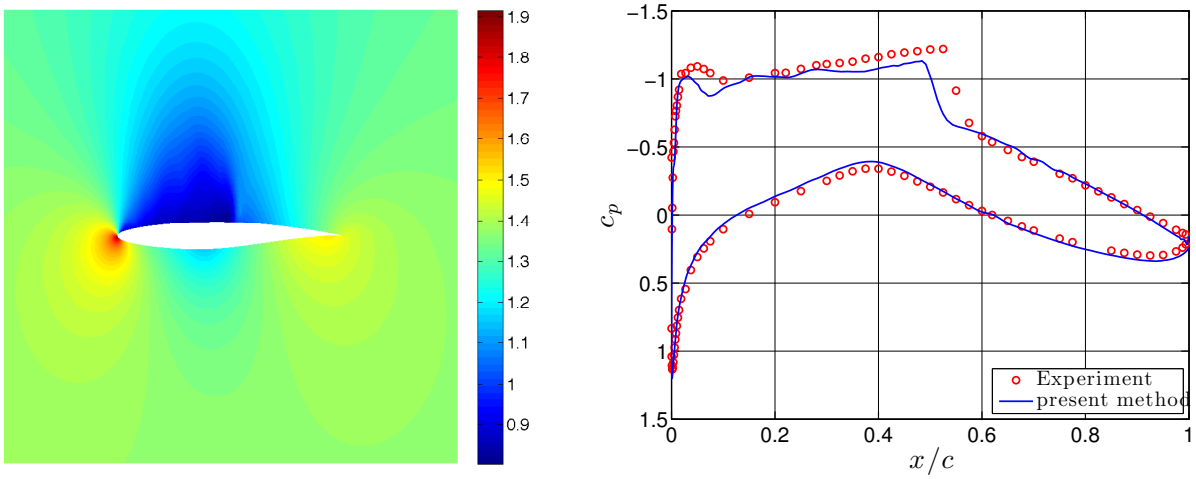

Figure 11: Pressure (left) and pressure coefficient distribution over airfoil surface (right) for turbulent transonic flow past RAE 2822 foil at $M_\infty = 0.729$, $\alpha = 2.31^o$, and $Re = 6.5 \times 10^6$.

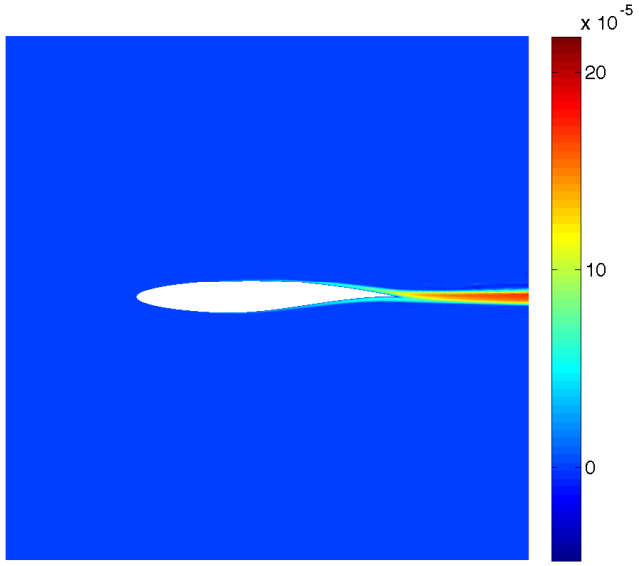

Figure 12: SA model working variable for the turbulent transonic flow past RAE 2822 foil at $M_\infty = 0.729$, $\alpha = 2.31^o$, and $Re = 6.5 \times 10^6$.

IV. Conclusion

We have presented a modification of the Spalart-Allmaras turbulence model suitable for high order computations on grids that are not well resolved at the edge of the boundary layer. Combined with forced transition terms and shock capturing the modified model has shown good stability properties on different instances.

Future extensions of this work would include a careful calibration of the constants in finer grids and the implementation of more robust solution strategies. Of particular interest would be a physically meaningful time stepping scheme that would allow free transition to be modeled if properly combined with a shear layer stability analysis tool.

Acknowledgments

J. Peraire and N. C. Nguyen would like to acknowledge the Singapore-MIT Alliance and the Air Force Office of Scientific Research under the MURI project on Biologically Inspired Flight for partially supporting this work. D. Moro would like to acknowledge the support of the Caja-Madrid Foundation for the Graduate Studies Scholarship that funded his work. The authors would like to thank A. Uranga for providing meshes and advice on some of the cases presented here.

References

[1]AGARD, *Experimental Data Base for Computer Program Assessment*, Report of the Fluid Dynamics Panel Working Group 04, AGARD-AR-138, May 1979.

[2]G. E. Barter and D. L. Darmofal. Shock capturing with PDE-based artificial viscosity for DGFEM: Part I. Formulation. *J. Comput. Phys.*, 229(5):1810–1827, 2010.

[3]F. Bassi, A. Crivellini, S. Rebay and M. Savini. Discontinuous Galerkin solution of the Reynolds Averaged Navier Stokes and kω turbulence model equations. *Computers and Fluids*, 34:507540, 2005

[4]F. Bassi, L. Botti, A. Colombo, A. Crivellini, N. Franchina, A. Ghidoni and S. Rebay. Very high-order accurate discontinuous Galerkin computation of transonic turbulent flows on aeronautical configurations. *ADIGMA A European Initiative on the Development of Adaptive Higher-Order Variational Methods for Aerospace Applications* edited by N. Kroll et al., NNFM 113, pp. 2538, Springer 2010.

[5]A. Bhagatwala and S.K. Lele. A modified artificial viscosity approach for compressible turbulence simulations. *Journal of Computational Physics*, 228(14):4965–4969, 2009.

[6]D. E. Coles and E. A. Hirst. Computation of Turbulent Boundary Layers. In *AFOSR-IFP-Stanford Conference, Vol. II*, Stanford University, CA, 1969.

[7]B. Cockburn, B. Dong, and J. Guzmán. A superconvergent LDG-hybridizable Galerkin method for second-order elliptic problems. *Math. Comp.*, 77:1887–1916, 2008.

[8]B. Cockburn, B. Dong, and J. Guzmán. A hybridizable and superconvergent discontinuous Galerkin method for biharmonic problems. *J. Sci. Comput.*, 40(1-3):141–187, 2009.

[9]B. Cockburn, B. Dong, J. Guzmán, M. Restelli, and R. Sacco. A hybridizable discontinuous galerkin method for steady-state convection-diffusion-reaction problems. *SIAM J. Scientific Computing*, 31(5):3827–3846, 2009.

[10]B. Cockburn and J. Gopalakrishnan. The derivation of hybridizable discontinuous Galerkin methods for Stokes flow. *SIAM J. Numer. Anal.*, 47:1092–1125, 2009.

[11]B. Cockburn, J. Gopalakrishnan, and R. Lazarov. Unified hybridization of discontinuous Galerkin, mixed and continuous Galerkin methods for second order elliptic problems. *SIAM J. Numer. Anal.*, 47:1319–1365, 2009.

[12]B. Cockburn, J. Gopalakrishnan, N.C. Nguyen, J. Peraire, and F.-J. Sayas. Analysis of HDG methods for Stokes flow. *Math. Comp.*, 80:723–760, 2011.

[13]B. Cockburn, J. Gopalakrishnan, and F.-J. Sayas. A projection-based error analysis of HDG methods. *Math. Comp.*, 79: 1351–1367, 2010.

[14]B. Cockburn, J. Guzmán, and H. Wang. Superconvergent discontinuous Galerkin methods for second-order elliptic problems. *Math. Comp.*, 78:1–24, 2009.

[15]B. Cockburn, N. C. Nguyen, and J. Peraire. A comparison of HDG methods for Stokes flow. *Journal of Scientific Computing*, 45(1-3):215–237, 2010.

[16]A. W. Cook. Artificial fluid properties for large-eddy simulation of compressible turbulent mixing. *Physics of Fluids*, 19(5):055–103, 2007.

[17]A. W. Cook and W. H. Cabot. A high-wavenumber viscosity for high-resolution numerical method. *Journal of Computational Physics*, 195(2):594–601, 2004.

[18]A. W. Cook and W. H. Cabot. Hyperviscosity for shockturbulence interactions. *Journal of Computational Physics*, 203(2):379–385, 2005.

[19]B. Fiorina and S K. Lele. An artificial nonlinear diffusivity method for supersonic reacting flows with shocks. *Journal of Computational Physics*, 222(1):246–264, 2007.

[20]Galbraith, M. and Visbal, M. Implicit Large-Eddy Simulation of low Reynolds number flow past the SD7003 airfoil. (AIAA P 2008-225). In *46th AIAA Aerospace Sciences Meeting and Exhibit* Reno, NV, January 2008

[21]R. Hartmann and P. Houston. Adaptive discontinuous Galerkin finite element methods for the compressible Euler equations. *J. Comput. Phys.*, 183:508–532, 2002.

[22]T. J. R. Hughes, M. Mallet, and A. Mizukami. A new finite element formulation for computational fluid dynamics: II. Beyond SUPG. *Comput. Methods Appl. Mech. Engrg.*, 54:341–355, 1986.

[23]A. Jameson. Analysis and design of numerical schemes for gas dynamics, 1: Artificial diffusion, upwind biasing, limiters and their effect on accuracy and multigrid convergence. *International Journal of Computational Fluid Dynamics*, 4:171–218, 1994.

[24]N. C. Nguyen, J. Peraire, and B. Cockburn. Hybridizable discontinuous Galerkin methods for the time-harmonic Maxwell's equations. *Journal of Computational Physics*. In Press.

[25]N. C. Nguyen, J. Peraire, and B. Cockburn. HDG methods for acoustics and elastodynamics: Superconvergence and postprocessing. *J. Comput. Phys.*, 230:3695–3718, 2011.

[26]N. C. Nguyen, J. Peraire, and B. Cockburn. An implicit high-order hybridizable discontinuous Galerkin method the incompressible Navier-Stokes equations. *J. Comput. Phys.*, 230:1147–1170, 2011.

[27]N. C. Nguyen, J. Peraire, and B. Cockburn. Hybridizable discontinuous Galerkin methods, *in Spectral and High Order Methods for Partial Differential Equations*, (Editors J. S. Hesthaven and E. M. Ronquist). *Lecture Notes in Computational Science and Engineering*, 2011, Volume 76, pages 63-84.

[28]N. C. Nguyen, J. Peraire, and B. Cockburn. An implicit high-order hybridizable discontinuous Galerkin method for linear convection-diffusion equations. *J. Comput. Phys.*, 228:3232–3254, 2009.

[29]N. C. Nguyen, J. Peraire, and B. Cockburn. An implicit high-order hybridizable discontinuous Galerkin method for nonlinear convection-diffusion equations. *J. Comput. Phys.*, 228:8841–8855, 2009.

[30]N. C. Nguyen, J. Peraire, and B. Cockburn. A hybridizable discontinuous Galerkin method for Stokes flow. *Comput. Methods Appl. Mech. Engrg.*, 199:582–597, 2010.

[31]N. C. Nguyen, J. Peraire, and B. Cockburn. A hybridizable discontinuous Galerkin method for the incompressible Navier-Stokes equations (AIAA Paper 2010-362). In *Proceedings of the 48th AIAA Aerospace Sciences Meeting and Exhibit*, Orlando, Florida, Janury 2010.

[32]N.C. Nguyen and J. Peraire, An adaptive shock-capturing HDG method for compressible flows presented at AIAA Conference, Hononulu, HI, June 2011.

[33]N. C. Nguyen, P. O. Persson, and J. Peraire, RANS Solutions using high order discontinuous Galerkin methods. In Proceedings of the 45th AIAA Aerospace Sciences Meeting and Exhibit, AIAA-2007-0914, Reno, NV, January 2007.

[34]J. Peraire, N. C. Nguyen, and B. Cockburn. A hybridizable discontinuous Galerkin method for the compressible Euler and Navier-Stokes equations (AIAA Paper 2010-363). In *Proceedings of the 48th AIAA Aerospace Sciences Meeting and Exhibit*, Orlando, Florida, Janury 2010.

[35]P. O. Persson and J. Peraire. Sub-cell shock capturing for discontinuous Galerkin methods. In Proceedings of the 44th AIAA Aerospace Sciences Meeting and Exhibit, AIAA-2006-112, Reno, NV, January 2006.

[36]S. Premasuthan, C. Liang, and A. Jameson. Computation of flows with shocks using spectral difference scheme with artificial viscosity (AIAA Paper 2010-1449). In *Proceedings of the 48th AIAA Aerospace Sciences Meeting and Exhibit*, Orlando, Florida, Janury 2010.

[37]H. Schlichting *Boundary-layer theory.* McGraw-Hil, New York, 1968

[38]P. Spalart and S. Allmaras A one-equation turbulence model for aerodynamic flows (AIAA Paper 92-0439). In *30th AIAA Aerospace Sciences Meeting*, Reno, USA, January 1992.

[39]S.-C. Soon, B. Cockburn, and H. K. Stolarski. A hybridizable discontinuous Galerkin method for linear elasticity. *International Journal for Numerical Methods in Engineering*, 80(8):1058–1092, 2009.

[40]E. Tadmor. Convergence of spectral methods for nonlinear conservation laws. *SIAM Journal on Numerical Analysis*, 26(1):30–44, 1989.

[41]A. Uranga, P.-O. Persson, M. Drela, and J. Peraire, Implicit Large Eddy Simulation of transition to turbulence at low Reynolds numbers using a Discontinuous Galerkin method. *International Journal for Numerical Methods in Engineering*, 87(1–5):232–261, 2011.